A Biquadratic Reflectance Model for Radiometric Image Analysis

Boxin Shi[1*] Ping Tan[2] Yasuyuki Matsushita[3] Katsushi Ikeuchi[1]
[1]The University of Tokyo [2]National University of Singapore [3]Microsoft Research Asia

Abstract

Radiometric image analysis methods heavily rely on reflectance models. Due to the complexity of real materials, methods based on simple models such as the Lambertian model often suffer from inaccuracy. On the other hand, more advanced models such as the Cook-Torrance model severely complicate the analysis problem. We tackle this dilemma by focusing on the low-frequency component of the reflectance. We propose a compact biquadratic reflectance model to represent the reflectance of a broad class of materials precisely in the low-frequency domain. We validate our model by fitting to both existing parametric models and non-parametric measured data, and show that our model outperforms existing parametric diffuse models. We show applications of reflectometry using general diffuse surfaces and photometric stereo for general isotropic materials. Experimental results show the effectiveness of our biquadratic model and its usefulness in radiometric image analysis.

1. Introduction

General surface reflectance is described by 4-D bidirectional reflectance distribution functions (BRDFs). Radiometric image analysis methods, including reflectometry and photometric shape analysis, rely on accurate modeling of reflectance. There has been a tremendous effort to build parametric BRDF models for realistic rendering (*e.g.*, [9, 36, 18, 3]). While these models are successful in graphics-rendering applications, they are seldom used in inverse problems in radiometric image analysis, because they often lead to highly nonlinear optimization problems. For the sake of computational simplicity and stability, the Lambertian model is still most widely used for inverse problems in spite of its limited accuracy in modeling real-world materials. To make the radiometric image analysis methods more accurate and reliable, a general yet simple parametric BRDF model is desired.

One of the key challenges in developing an analytic BRDF model is accurately modeling specular reflections that exhibit high-frequency variations. Modeling high-frequency specular reflections is crucial for photo-realistic rendering in computer graphics. However, it is seldom necessary for inverse problems in computer vision like photometric stereo. Instead, the low-frequency component is more actively used in radiometric analysis, because its dense observation provides a reliable source for the analysis problem[1]. Motivated by this observation, we develop a new analytic reflectance model for radiometric image analysis. This model relies on a *biquadratic* representation for accurately modeling the low-frequency component while neglecting the high-frequency component. Although it excludes strong specularities including specular spikes, it can represent broad and smooth specular lobes as well as the diffuse component.

Our biquadratic representation uses a factorized form of the bivariate BRDF model [29], *i.e.*, the product of half- and difference-angle terms as $\rho(\theta_h, \theta_d) \simeq \rho_1(\theta_h)\rho_2(\theta_d)$. We use a quadratic function for each term to achieve a compact parameterization. This representation is well suited for the low-frequency component of isotropic BRDFs as we will see in the experimental results, and it is more precise than the Lambertian model, existing parametric models with general diffuse terms [18, 3] and specular terms [9, 36]. In addition, because of its compactness, model estimation becomes tractable for inverse problems in radiometric image analysis. As applications of the proposed model, we show its usages in reflectometry for general diffuse surfaces and photometric stereo for general isotropic materials.

2. Related Works

Various parametric BRDF models have been developed over the decades. These can be categorized into physically-based and empirical models. The former group includes microfacet-based models, such as the Torrance-Sparrow [35] and Cook-Torrance [9] models for specular surfaces, and the Oren-Nayar model [25] for diffuse surfaces. On the other hand, empirical models, such as the Phone [26], Blinn-Phong [4], and Lafortune models [18],

*Part of this work was done while the first author was visiting National University of Singapore.

[1]For example, strong specular spikes (high-frequency) are observed only when the surface normal coincides with the bisector of viewing and lighting directions.

use generic functions to express BRDFs. Some models bridge these two categories by partly using physically motivated terms, *e.g.*, the Ward [36] and Ashikhmin models [3]. An experimental evaluation of various models can be found in [23]. Generally, parametric models are compact and easy to use for forward problems, but they are often designed for a limited class of materials.

A BRDF can also be naturally represented in a non-parametric form by a 4-D discrete table of densely measured data. This can be simplified to a 3-D table if the materials are isotropic [11, 20, 21]. It can be further reduced to a 2-D table for a wide range of isotropic reflectances [27, 2, 28]. Although high-quality rendering can be achieved using measured data, the non-parametric form is generally unsuitable for inverse problems because its large number of parameters complicate the problem. There are recent efforts that efficiently represent the BRDFs using non-parametric [40], semi-parametric [7], or parametric [24] forms to achieve high modeling accuracy by employing different basis functions. Our goal shares a similar spirit, but we focus on modeling the low-frequency reflectance using a simpler parametric form with an emphasis on radiometric image analysis.

Radiometric image analysis. Radiometric image analysis seeks to recover scene properties, such as reflectance or shape, from recorded scene radiance. Here we briefly review related works in reflectometry and photometric stereo.

Most of the works on reflectometry are based on parametric reflectance models, such as [39, 5, 14], with exceptions of [27, 28], which assume non-parametric bivariate BRDFs and adopt a discrete table representation. All these methods focus on reflectance estimation assuming a known shape with different input: multiple input images under a moving point light source [39, 14], a single input image with known [5, 27] or unknown environment illumination [28]. A successful reflectometry requires both an accurate reflectance model and a reliable model estimation method.

In the shape estimation context, early photometric stereo works [37, 32] are based on the Lambertian reflectance model. To handle real surfaces that are often non-Lambertian, some algorithms attempt to discard the non-Lambertian reflectance as outliers [38]. The others employ parametric reflectance models, such as the Torrance-Sparrow model [12], the Ward model [8, 13], and other multi-lobe models [33].

There are more recent approaches that attempt to solve the photometric stereo problem with reflectance symmetries, such as isotropy and reciprocity [1, 2, 34, 6], without using a strong assumption on reflectance. Photometric stereo can also be applied to surfaces with general reflectance by using thousands of images [16], or considering some consensus properties [15]. We study photometric stereo based on our biquadratic reflectance model. Since our reflectance model is compact yet accurate for many real materials, our method requires simple data capturing and optimization.

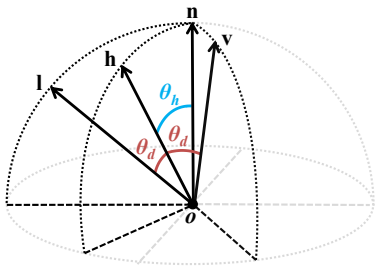

Figure 1. The definitions of θ_h and θ_d.

3. Biquadratic Reflectance Model

We denote $\mathbf{n}$ as a unit surface normal, $\mathbf{h}$ as the bisector of lighting direction $\mathbf{l}$ and viewing direction $\mathbf{v}$, *i.e.*, $\mathbf{h} = (\mathbf{l}+\mathbf{v})/\|\mathbf{l}+\mathbf{v}\|$. Following [29], we use θ_h to denote the angle between $\mathbf{n}$ and $\mathbf{h}$, and θ_d for the angle between $\mathbf{l}$ (or $\mathbf{v}$) and $\mathbf{h}$ as illustrated in Fig. 1. Hence, the following relationships hold: $\mathbf{n}^T\mathbf{h} = \cos\theta_h$ and $\mathbf{l}^T\mathbf{h} = \cos\theta_d$.

Our reflectance model is based on the bivariate BRDF model [29], which shows that most of the isotropic BRDFs can be represented as a bivariate function $\rho(\theta_h, \theta_d)$. This representation is evaluated by [27] with a large number of measured BRDFs [21] in the development of passive reflectometry. It is further discussed in [29] that any isotropic BRDF based on microfacet theory should consist of a univariate function of θ_h, and its Fresnel term should be a univariate function of θ_d. As shown by [3], the masking and shadowing terms in a microfacet-based BRDF model vary smoothly and are actually close to constant. These analyses motivate us to further simplify the bivariate function $\rho(\theta_h, \theta_d)$ as a factorized form $\rho_1(\theta_h)\rho_2(\theta_d)$. Similar simplification has been used in [19] to assist material capturing and editing.

To obtain a compact parametric model suitable for inverse problems, we make a further simplification by representing the factorized terms as quadratic functions of $\cos\theta_h$ and $\cos\theta_d$. As a result, our BRDF model becomes a biquadratic function. As we will see later, the proposed biquadratic model can represent a wide class of low-frequency BRDFs and has a computationally tractable form in radiometric image analysis.

Based on these discussions, we define a biquadratic reflectance model for isotropic low-frequency reflectance as the following:

$$\begin{aligned}\rho(\theta_h, \theta_d) \simeq & \rho_1(\theta_h)\rho_2(\theta_d) = \tilde{\rho_1}(\mathbf{n}^T\mathbf{h})\tilde{\rho_2}(\mathbf{l}^T\mathbf{h}) \\ = & \big(A_1(\mathbf{n}^T\mathbf{h})^2 + B_1(\mathbf{n}^T\mathbf{h}) + C_1\big) \\ & \big(A_2(\mathbf{l}^T\mathbf{h})^2 + B_2(\mathbf{l}^T\mathbf{h}) + C_2\big).\end{aligned} \tag{1}$$

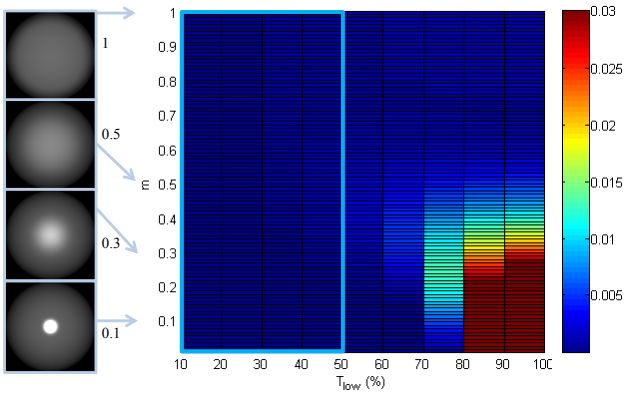

Figure 2. BRDF fitting errors of our model to the Cook-Torrance model. The columns vary with T_{low} and the rows vary with m in the Cook-Torrance model. Some rendered images are displayed on the left side for reference.

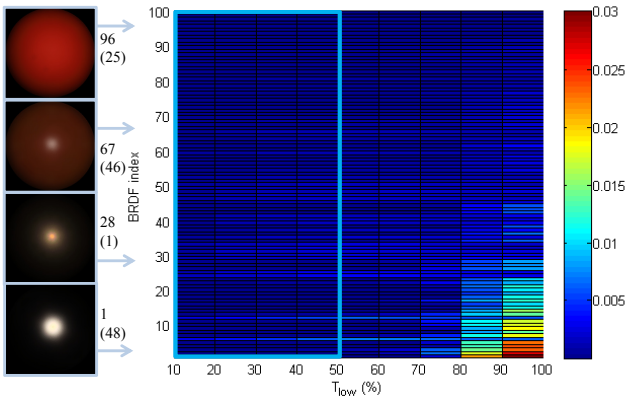

Figure 3. BRDF fitting errors of our model to the 100 materials in the MERL database. The columns vary with T_{low}, and the rows represent different BRDFs with indices ordered by the mean fitting errors over columns. Some rendered images are displayed on the left for reference, with reordered BRDF indices (the numbers in brackets are their original indices in the database) aside.

In practice, to simplify model fitting, the biquadratic form of Eq. (1) can be further relaxed as

$$\begin{aligned}\tilde{\rho}(x,y) =& Ax^2y^2 + Bx^2y + Cx^2 + Dxy^2 + Exy + \\ & Fx + Gy^2 + Hy + I,\end{aligned} \tag{2}$$

where $x = \mathbf{n}^T\mathbf{h}$, $y = \mathbf{l}^T\mathbf{h}$ are defined for notation simplicity. There are 9 parameters in total, and we denote them in a vector form as $\mathbf{x} = [A, B, \cdots, I]^T \in \mathbb{R}^{9\times 1}$. Note that the conversion from Eq. (1) to Eq. (2) is unique, but the other direction is not, and Eq. (2) may not always have the product form of Eq. (1). Eq. (2) is a linear function of its parameters A to I, while Eq. (1) is a bilinear function of these parameters. Hence, the relaxed model is much easier to fit.

3.1. Model Validation

Intuitively, our model can accurately represent the low-frequency part of conventional dichromatic reflectance models [31], which represent reflectances as a summation of Lambertian diffuse and specular terms. Since the specular term is mostly concentrated in the high-frequency part, the low-frequency Lambertian term can be well represented by our model with $A_1 = B_1 = A_2 = B_2 = 0$. Our model can also represent the low-frequency component of BRDF models that rely only on $\mathbf{n}^T\mathbf{h}$, such as the Blinn-Phong model [4]. The low-frequency part of these models can be approximated by our model with $A_2 = B_2 = 0$.

In the following, we assess the modeling accuracy of our biquadratic reflectance model by fitting existing parametric models and measured data. We use a simple intensity thresholding to separate low-frequency and high-frequency reflectances, since high-frequency (strong specular) reflectances generally show high intensity. We further compare our biquadratic model with existing parametric models.

Fitting to parametric BRDFs. The Cook-Torrance model [9] is widely used to represent surface reflectance. It consists of a Lambertian diffuse and a specular term. The specular component is modeled as a multiplication of microfacet distribution D, the Fresnel term F and the geometrical attenuation term G. The microfacet distribution D is represented as

$$D = \frac{1}{4m^2(\mathbf{n}^T\mathbf{h})^4}\exp\left(\frac{1}{m^2}\left(1 - \frac{1}{(\mathbf{n}^T\mathbf{h})^2}\right)\right), \tag{3}$$

where m indicates the surface roughness. D is clearly a function of θ_h. F is often simplified by the Schlick's approximation [30, 3], denoted as

$$F = \rho_s + (1 - \rho_s)(1 - \mathbf{l}^T\mathbf{h})^5, \tag{4}$$

where ρ_s is a constant. Hence, F is a function of θ_d. Although the term G is relatively complicated, it varies smoothly and is close to constant over a large range of exitant angles as evaluated in [22, 3]. Therefore, $\rho_1(\theta_h)\rho_2(\theta_d)$ is a good approximation for the Cook-Torrance model. Other models based on the microfacet theory, such as the Ward [36] model, have similar expressions.

For an experimental validation, we fit our biquadratic model to synthetic data generated by the Cook-Torrance model with varying surface roughness. The relative strength of diffuse and specular components is fixed to 1. We fix the viewing direction at $(0, 0, 1)$ and sample 1620 normal directions from the visible hemisphere by uniformly choosing 36 longitudes and 45 altitudes. We then randomly sample 100 light directions to calculate the reflected radiance. For each normal direction under varying lightings, we sort the radiance intensities in an increasing order and select only those non-shadowed samples that are ranked below a predefined

percentage T_{low}. We then fit our biquadratic model to these selected samples in a least-squares manner. Specifically, we fit Eq. (2) by a linear least-squares and use its results as initial values to fit Eq. (1) in an iterative manner. At each iteration, we fix the parameters of one quadratic function and optimize the other parameters by a linear least-squares. It usually takes no more than 10 iterations to converge. This process is repeated with different surface roughness m and different T_{low}.

The color encoded mean absolute errors (MAE) of the fitting are summarized in Fig. 2 in a matrix form with varying m and T_{low}. Note that reflectance with a large roughness value has a broad specular lobe, which is mixed with the Lambertian diffuse reflectance to form the low-frequency reflectance. From the region within the light blue rectangle in Fig. 2, we conclude that our model well fits the low-frequency reflectance of the Cook-Torrance model with different roughnesses.

Fitting to measured data. We also assess our biquadratic model by fitting to synthetic data generated from measured MERL BRDF database [21]. The input samples are generated in the same way as the previous experiment, except that we use the measured BRDFs instead of the Cook-Torrance model. The MAE values are shown in Fig. 3. Note that the rows indicate different BRDFs in the database now. Similar to Fig. 2, our model fits well to the low-frequency reflectance of different materials, and our model has smaller fitting errors for materials with broader specular lobes.

3.2. Comparison with Other Parametric Models

Models with general diffuse terms. There are existing parametric models with general diffuse terms, such as the Lafortune and the Ashikhmin[2] models.

In the Lafortune model [18], a general rotationally symmetric diffuse component ρ_L is written as

$$\rho_L = C_d \left(\mathbf{n}^T\mathbf{l}\right)^k \left(\mathbf{n}^T\mathbf{v}\right)^k, \quad (5)$$

where C_d and k are model parameters. The general diffuse term of Ashikhmin model [3] ρ_A is defined as

$$\rho_A = R\left(1-\left(1-\frac{\mathbf{n}^T\mathbf{l}}{2}\right)^5\right)\left(1-\left(1-\frac{\mathbf{n}^T\mathbf{v}}{2}\right)^5\right), \quad (6)$$

where R is the model parameter.

Models with specular terms. Several parametric models assume a Lambertian diffuse term and use a microfacet-based specular component, such as the Cook-Torrance and Ward models. These models can be represented as

$$\rho_S = \frac{k_d}{\pi} + k_s S(\mathbf{n}, \mathbf{l}, \mathbf{v}, m), \quad (7)$$

[2]In this paper, we only consider the general diffuse terms of these two models.

where k_d and k_s are model parameters representing the strength of diffuse and specular terms respectively; S is a nonlinear function with m as another model parameter. In the Cook-Torrance model, m is encoded in the D term in Eq. (3) and the Ward model has a similar expression.

Fitting comparison. We again use the MERL BRDF database for evaluation by setting the threshold $T_{low} = 25\%$ to extract the low-frequency reflectance. Fitting Eq. (6) is straightforward. For fitting Eq. (5), we take logarithm of both sides of the equation and estimate the log-parameters by a linear least-squares. For fitting Eq. (7), we adopt the similar strategies as [23], and use the Matlab function "lsqnonlin" to solve the nonlinear optimization. The fitting errors are shown in Fig. 4, where "biquadratic (relax.)" and "biquadratic (iter.)" indicate the relaxed model in Eq. (2) and the original model in Eq. (1), respectively.

Compare to existing general diffuse terms, our model has a smaller fitting error than the Lafortune and Ashikhmin models. Though with specular components included, the Cook-Torrance and Ward models cannot outperform our model in fitting the low-frequency reflectance. Besides, our model has a simpler analytic form, which makes it easier to use in inverse problems. The errors of "biquadratic (relax.)" and "biquadratic (iter.)" are very similar. It suggests the relaxed model is a good replacement for the original biquadratic model when computational efficiency is important.

3.3. Why Biquadratic?

$\tilde{\rho}_1(x)$ and $\tilde{\rho}_2(y)$ might also be represented by polynomials of any orders, *e.g.*, linear or cubic. We choose to represent both of them by quadratic functions to achieve a good trade-off between modeling accuracy and model complexity. We compare the accuracy of bilinear, biquadratic, and bicubic models in Fig. 4. The bilinear model is less accurate than the Lafortune model. On the other hand, the bicubic model has the smallest fitting error, because its higher degrees of freedom. However, as we will see in the photometric stereo application, its cubic function of $\mathbf{n}$ complicates the normal estimation. Therefore, we choose the biquadratic model.

4. Application to Reflectometry

Although our biquadratic model mainly intends to model the low-frequency reflectance, it can also be used as an empirical reflectance model for materials without significant specular spikes. With our model in Eq. (2), reflectometry becomes a simple linear problem $\mathbf{A}\mathbf{x} = \mathbf{i}$, where $\mathbf{i}$ records radiance values. For each observation, we can calculate the (x, y) terms (a 9-D row vector) according to Eq. (2) from $\mathbf{n}$, $\mathbf{l}$, and $\mathbf{v}$ when the shape and lighting are all calibrated. From p samples ($p \geqslant 9$) that are linearly independent, the matrix $\mathbf{A} \in \mathbb{R}^{p\times 9}$ and observations $\mathbf{i} \in \mathbb{R}^{p\times 1}$ are obtained.

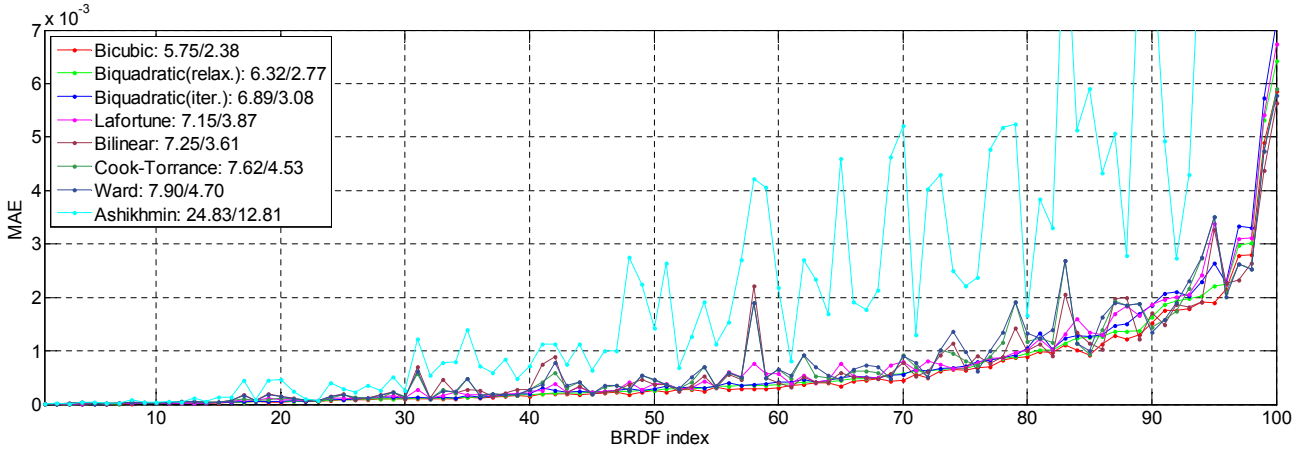

Figure 4. BRDF fitting errors. The Y-axis shows the MAE values. The X-axis shows BRDF indices ordered by the fitting errors of "biquadratic (relax.)" for visualization purpose. The mean/median MAEs ($\times 10^{-4}$) over the BRDF index are shown in the legend.

The model parameters $\mathbf{x}$ can be determined by simply solving the linear system as $\mathbf{x} = (\mathbf{A}^T\mathbf{A})^{-1}\mathbf{A}^T\mathbf{i}$. For a curved surface with a single material, a single image under a point light source provides sufficient information for reflectometry.

To verify the method, we pick some materials (*e.g.*, BLUE-RUBBER, DARK-RED-PAINT, YELLOW-PAINT, *etc.*), which do not show strong specularities from the MERL BRDF database. We synthesize a single image of a sphere under a point light source as input and fit our model to it. All the tested materials show the similar results with an average MAE about 8×10^{-4}. Here we show the BLUE-RUBBER example in Fig. 5. The left most is the original input image. The others are images rendered according to the reflectance model estimated from the input image. We also show the comparison with the bivariate model [27] and the Lambertian model. The bivariate model is generated similarly as [27] by taking one slice of the 3-D discrete BRDF table ($\rho(\theta_h, \theta_d, \phi_d)$) and averaging over ϕ_d (the rotation of difference-angle). Although our model performs slightly worse than the bivariate model, we have significantly fewer parameters. In contrast, the simple Lambertian model generates the largest error. Generally, our model bears relatively larger errors when high-frequency reflectance appears (*e.g.*, center of the sphere), since it only models low-frequency reflectance.

We also use real data to evaluate our method. The input image is captured from a ping pong ball. For visual validation, we show a sphere rendered according to the biquadratic model, the Lafortune model and the Lambertian model estimated from this input image in the lower part of Fig. 5. The result here is consistent with the BRDF fitting results in Fig. 4. Our model can better describe the low-frequency reflectance than the Lafortune and Lambertian models.

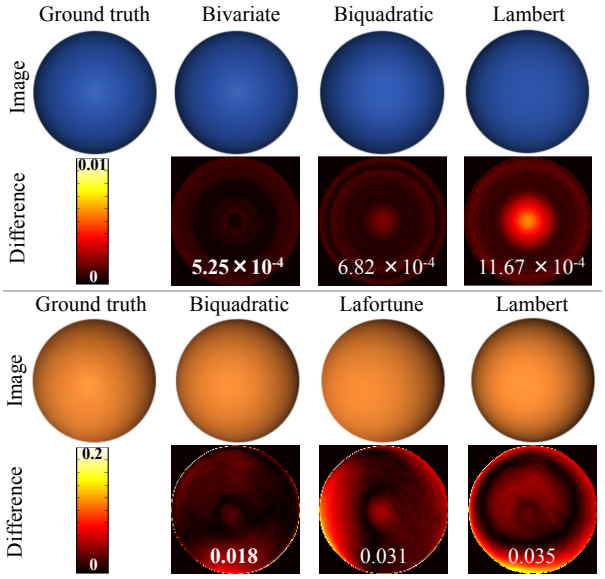

Figure 5. A synthetic and a real-world results of reflectometry. Below the rendered (captured) spheres we show the difference maps w.r.t. the ground truth and their MAEs.

5. Application to Photometric Stereo

In this section, we apply our biquadratic reflectance model to photometric stereo to recover surface normals from images captured from a fixed camera under varying lightings. We assume an orthographic camera and directional lightings. The camera-centered coordinate system is chosen such that $\mathbf{v} = (0, 0, 1)^T$. We fit our biquadratic reflectance model at each pixel independently, thus this approach can handle spatially varying BRDFs.

5.1. Algorithm Detail

From the photometric stereo images, we observe multiple radiance intensities at each pixel. For each pixel, we first use a very small intensity threshold to skip shadows. And then we sort remaining observations in increasing order and

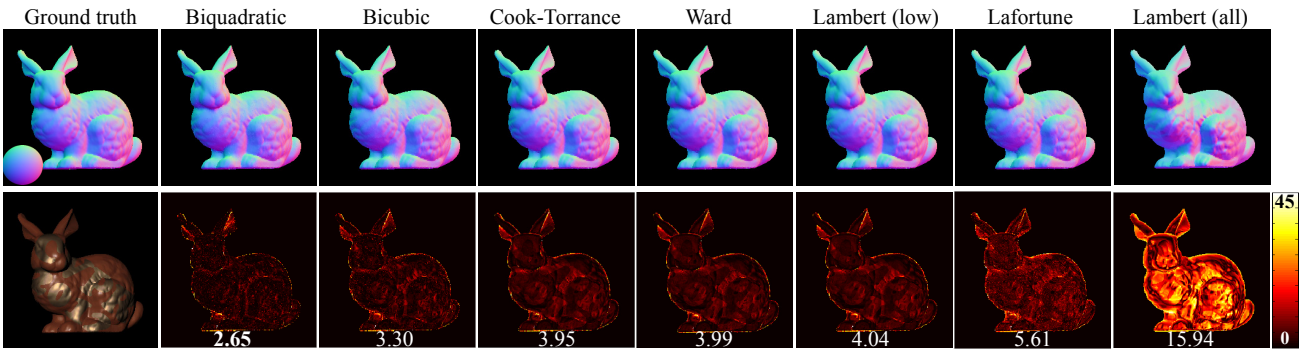

Figure 6. Photometric stereo with synthetic data. One of the input images is given under the ground truth normal map. Below other normal maps are angular difference maps w.r.t. the ground truth. The numbers on the difference maps show mean angular errors (degree) of normal estimates.

only keep those ranked below a percentage T_{low}, which is empirically determined within $[20\%, 40\%]$. We use $\mathbf{i}_{low}$ to denote the concatenated vector of these remaining observations and stack their corresponding lighting directions to from a matrix $\mathbf{L}_{low}$. We then obtain the following equation:

$$\mathbf{i}_{low} = \bar{\rho}(\mathbf{n}, \mathbf{L}_{low}) \circ (\mathbf{n}^T \mathbf{L}_{low}), \tag{8}$$

where '$\circ$' indicates element-wise multiplication. $\bar{\rho}(\cdot,\cdot)$ encodes the reflectance parameter $\mathbf{x}$ in the same manner as $\tilde{\rho}(\cdot,\cdot)$ in Eq. (2), but operates on each $\mathbf{n}$ and $\mathbf{l}$. We use the relaxed biquadratic model of Eq. (2) for better computational efficiency. The surface normal $\mathbf{n}$ and the BRDF parameters $\mathbf{x}$ can be determined by iteratively optimizing the following objective function:

$$(\mathbf{n}^*, \mathbf{x}^*) = \underset{\mathbf{n},\mathbf{x}}{\operatorname{argmin}} \|\bar{\rho}(\mathbf{n}, \mathbf{L}_{low}) \circ (\mathbf{n}^T \mathbf{L}_{low}) - \mathbf{i}_{low}\|^2. \tag{9}$$

At each iteration, we first fix the normal direction $\mathbf{n}$ and refine $\mathbf{x}$ by a linear least-squares. We then substitute $\mathbf{x}$ and $\mathbf{n}$ to determine $\bar{\rho}(\cdot,\cdot)$. Once $\bar{\rho}(\cdot,\cdot)$ is calculated, we update $\mathbf{n}$ again by a linear least-squares. To initialize this iterative optimization, we first apply Lambertian photometric stereo [37] with $\mathbf{i}_{low}$ and $\mathbf{L}_{low}$ to estimate an initial normal. The iterative optimization stops when the residual of Eq. (9) does not change. In our implementation, we stop it when the change becomes less than 10^{-7}.

This same approach can be applied for other analytic BRDF models, such as the Lafortune, Cook-Torrance and Ward models. However, when it is used, the estimation of their BRDF parameters by fixing $\mathbf{n}$ becomes highly nonlinear. Similarly, though we might use higher-order polynomials such as cubic functions to represent $\tilde{\rho}_1(x)$ and $\tilde{\rho}_2(y)$, high-order polynomials are prone to different instabilities (numerical errors, Runge's phenomenon [10], *etc.*). Hence, the biquadratic representation is a good trade-off between model complexity and accuracy.

5.2. Experiments

Spatially varying BRDFs. We generate synthetic images with spatially varying BRDFs to quantitatively verify our photometric stereo method. We mix ALUM-BRONZE and CHERRY-235 from the MERL BRDF database on a BUNNY model, and render 100 images as input. We still set $T_{low} = 25\%$ for this synthetic data. We use the same solution method as Sec. 5.1, and replace $\bar{\rho}(\cdot,\cdot)$ as bicubic, Lafortune, Cook-Torrance and Ward models respectively to make a comparison. The estimated normal maps[3] and their angular errors are shown in Fig. 6.

The traditional Lambertian photometric stereo with all images ("Lambert (all)") [37] fails on those materials with complicated reflectances (*e.g.*, the texture boundaries on BUNNY is clearly visible in the error map). By only focusing on the low-frequency reflectance, photometric stereo can work reasonably well on general reflectance even with the Lambertian model ("Lambert (low)"). Further by fitting the low-frequency reflectance with our biquadratic model, the estimated normals become even more accurate. Compared with other BRDF models, the mean error from the bicubic case is larger than the biquadratic case due to the high-order polynomial fitting, and the errors from the Cook-Torrance, Ward and Lafortune models are larger than our model partly due to their lower modeling ability for low-frequency reflectance. Besides, the nonlinear reflectance might cause the iterative optimization performs poor, which makes the Lafortune case has a larger error than the "Lambert (low)" case.

Real-world data. We show the results of real-world data in Fig. 7. For an easy reference, we refer to these examples as (from top to bottom row) GOURD1 (102), GOURD2 (98), APPLE (112), POST (91) and TEAPOT (73), with the number of input images in the bracket. The first three datasets are recorded by Alldrin *et al.* [2]. Others are captured by ourselves with a Sony XCD-X710CR camera. We do not carefully control exposure to avoid saturation, since our method can naturally skip undesired strong specular and saturation regions by setting T_{low}. These objects include various chal-

[3] x, y, z components of surface normal are linearly mapped to the R, G, B channels.

lenging materials for photometric stereo, such as porcelain and shiny plastic.

In Fig. 7, the left column shows one of the input images to the photometric stereo algorithm and a reference image (not used in calculation) of the same object under natural lighting and a new view point[4]. The middle and right columns show the estimated surface normal and integrated surfaces using our method and the Lambertian photometric stereo. The integrated surfaces are produced by the shapelet surface reconstruction method [17]. The recovered surfaces are aligned to the reference views for making qualitative evaluation, and our reconstruction agrees well with them.

6. Conclusion

We present a biquadratic reflectance model for low-frequency reflectance of isotropic surfaces. Our model can represent a broad class of real materials at high precision while retaining sufficient simplicity for radiometric image analysis. Extensive experiments using both synthetic and measured data demonstrate its effectiveness in modeling low-frequency BRDF components. We further show that it can be used for reflectometry to capture general diffuse reflectance. We also propose a novel photometric stereo solution to general isotropic materials using the proposed reflectance model. These applications show the applicability of our model in radiometric image analysis.

The current model is limited to isotropic materials. We also hope to analyze the characteristics of the low-frequency component of anisotropic reflectance and extend our biquadratic model to a wider variety of reflectances. At the same time, currently the low-frequency reflectance is identified by a simple intensity threshold. How to detect it in a more principled manner is also left as our future work.

Acknowledgement

B. Shi and K. Ikeuchi was partially supported by the Digital Museum Project, Ministry of Education, Culture, Sports, Science & Technology in Japan. P. Tan was supported by the Singapore ASTAR grant R-263-000-592-305 and MOE grant R-263-000-555-112.

References

[1] N. Alldrin and D. Kriegman. Toward reconstructing surfaces with arbitrary isotropic reflectance: A stratified photometric stereo approach. In *Proc. of International Conference on Computer Vision (ICCV)*, 2007.

[2] N. Alldrin, T. Zickler, and D. Kriegman. Photometric stereo with non-parametric and spatially-varying reflectance. In *Proc. of IEEE Conference on Computer Vision and Pattern Recognition (CVPR)*, 2008.

[3] M. Ashikhmin and P. Shirley. An anisotropic Phong BRDF model. *Journal of Graphics Tools*, 5(2):25–32, 2000.

[4] J. Blinn. Models of light reflection for computer synthesized pictures. In *Proc. of ACM SIGGRAPH*, 1977.

[4]For Alldrin's data, we use the rendered results from their paper [2].

[5] S. Boivin and A. Gagalowicz. Image-based rendering of diffuse, specular and glossy surfaces from a single image. In *Proc. of ACM SIGGRAPH*, 2001.

[6] M. Chandraker, J. Bai, and R. Ramamoorthi. A theory of photometric reconstruction for unknown isotropic reflectances. In *Proc. of IEEE Conference on Computer Vision and Pattern Recognition (CVPR)*, 2011.

[7] M. Chandraker and R. Ramamoorthi. What an image reveals about material reflectance. In *Proc. of International Conference on Computer Vision (ICCV)*, 2011.

[8] H. Chung and J. Jia. Efficient photometric stereo on glossy surfaces with wide specular lobes. In *Proc. of IEEE Conference on Computer Vision and Pattern Recognition (CVPR)*, 2008.

[9] R. Cook and K. Torrance. A reflectance model for computer graphics. *ACM Trans. on Graph.*, 1(1):7–24, 1982.

[10] G. Dahlquist and A. Bjork. 4.3.4. Equidistant interpolation and the Runge phenomenon. *Numerical Methods*, pages 101–103, 1974.

[11] K. Dana, B. van Ginneken, S. Nayar, and J. Koenderink. Reflectance and texture of real world surfaces. *ACM Trans. on Graph.*, 18(1):1–34, 1999.

[12] A. Georghiades. Incorporating the Torrance and Sparrow model of reflectance in uncalibrated photometric stereo. In *Proc. of International Conference on Computer Vision (ICCV)*, 2003.

[13] D. Goldman, B. Curless, A. Hertzmann, and S. Seitz. Shape and spatially-varying BRDFs from photometric stereo. *IEEE Trans. Pattern Anal. Mach. Intell.*, 32(6):1060–1071, 2010.

[14] K. Hara, K. Nishino, and K. Ikeuchi. Mixture of spherical distributions for single-view relighting. *IEEE Trans. Pattern Anal. Mach. Intell.*, 30(1):25–35, 2008.

[15] T. Higo, Y. Matsushita, and K. Ikeuchi. Consensus photometric stereo. In *Proc. of IEEE Conference on Computer Vision and Pattern Recognition (CVPR)*, 2010.

[16] M. Holroyd, J. Lawrence, G. Humphreys, and T. Zickler. A photometric approach for estimating normals and tangents. In *ACM Trans. on Graph. (Proc. of SIGGRAPH Asia)*, 2008.

[17] P. Kovesi. Shapelets correlated with surface normals produce surfaces. In *Proc. of International Conference on Computer Vision (ICCV)*, 2005.

[18] E. Lafortune, S. Foo, K. Torrance, and D. Greenberg. Non-linear approximation of reflectance functions. In *Proc. of ACM SIGGRAPH*, 1997.

[19] J. Lawrence, A. Ben-Artzi, C. DeCoro, W. Matusik, H. Pfister, R. Ramamoorthi, and S. Rusinkiewicz. Inverse shade trees for non-parametric material representation and editing. In *ACM Trans. on Graph. (Proc. of SIGGRAPH)*, 2006.

[20] S. Marschner, S. Westin, E. Lafortune, K. Torrance, and D. Greenberg. Image-based BRDF measurement including human skin. In *Proc. of Eurographics Symposium on Rendering*, pages 139–152, 1999.

[21] W. Matusik, H. Pfister, M. Brand, and L. McMillan. A data-driven reflectance model. In *ACM Trans. on Graph. (Proc. of SIGGRAPH)*, 2003.

[22] S. Nayar, K. Ikeuchi, and T. Kanade. Surface reflection: Physical and geometrical perspectives. *IEEE Trans. Pattern Anal. Mach. Intell.*, 13(7):611–634, 1991.

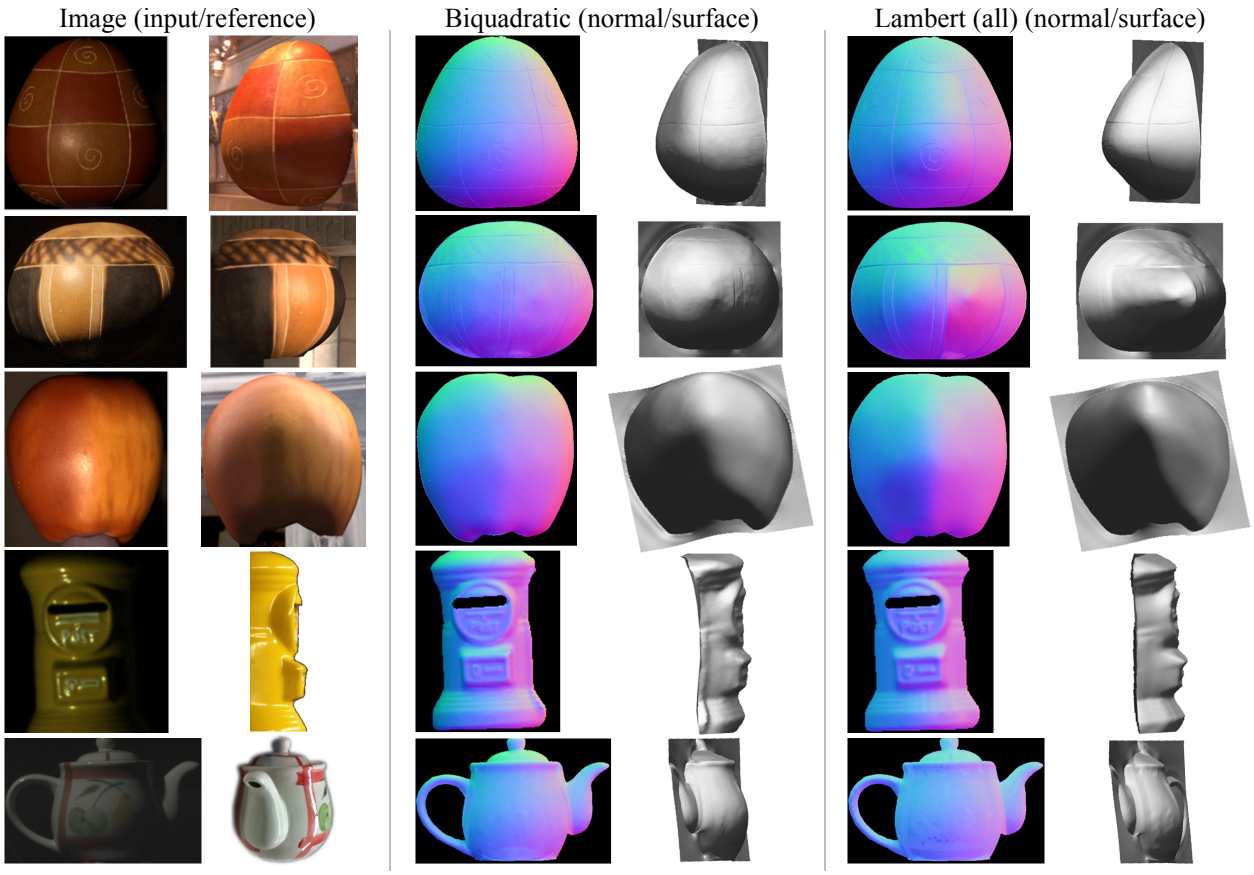

Figure 7. Photometric stereo with real-world data. Courtesy of Alldrin *et al*. [2] for the top three data.

[23] A. Ngan, F. Durand, and W. Matusik. Experimental analysis of BRDF models. In *Proc. of Eurographics Symposium on Rendering*, 2005.

[24] K. Nishino. Directional statistics BRDF model. In *Proc. of International Conference on Computer Vision (ICCV)*, 2009.

[25] M. Oren and S. Nayar. Diffuse reflectance from rough surfaces. In *Proc. of IEEE Conference on Computer Vision and Pattern Recognition (CVPR)*, 1993.

[26] B. Phong. Illumination for computer generated pictures. In *Proc. of ACM SIGGRAPH*, 1975.

[27] F. Romeiro, Y. Vasilyev, and T. Zickler. Passive reflectometry. In *Proc. of European Conference on Computer Vision (ECCV)*, 2008.

[28] F. Romeiro and T. Zickler. Blind reflectometry. In *Proc. of European Conference on Computer Vision (ECCV)*, 2010.

[29] S. Rusinkiewicz. A new change of variables for efficient BRDF representation. In *Rendering Techniques (Proc. of Eurographics Workshop on Rendering)*, 1998.

[30] C. Schlick. An inexpensive BRDF model for physically-based rendering. *Computer Graphics Forum*, 13(3):233–246, 1994.

[31] S. Shafer. Using color to separate reflection components. *Color Research*, 10(4):210–218, 1985.

[32] W. Silver. Determining shape and reflectance using multiple images. *Master's thesis, MIT*, 1980.

[33] P. Tan, S. Lin, and L. Quan. Subpixel photometric stereo. *IEEE Trans. Pattern Anal. Mach. Intell.*, 30(8):1460–1471, 2008.

[34] P. Tan, L. Quan, and T. Zickler. The geometry of reflectance symmetries. *IEEE Trans. Pattern Anal. Mach. Intell.*, 33(12):2506–2520, 2011.

[35] K. Torrance and E. Sparrow. Theory for off-specular reflection from roughened surfaces. *Journal of the Optical Society of America*, 57(9):1105–1114, 1967.

[36] G. Ward. Measuring and modeling anisotropic reflection. *Computer Graphics*, 26(2):265–272, 1992.

[37] R. Woodham. Photometric method for determining surface orientation from multiple images. *Optical Engineering*, 19(1):139–144, 1980.

[38] L. Wu, A. Ganesh, B. Shi, Y. Matsushita, Y. Wang, and Y. Ma. Robust photometric stereo via low-rank matrix completion and recovery. In *Proc. of Asian Conference on Computer Vision (ACCV)*, 2010.

[39] Y. Yu, P. Debevec, J. Malik, and T. Hawkins. Inverse global illumination: Recovering reflectance models of real scenes from photographs. In *Proc. of ACM SIGGRAPH*, 1999.

[40] T. Zickler, R. Ramamoorthi, S. Enrique, and P. Belhumeur. Reflectance sharing: Predicting appearance from a sparse set of images. *IEEE Trans. Pattern Anal. Mach. Intell.*, 28(8):1287–1302, 2006.